Doxycycline has Distinct Apicoplast-Specific Mechanisms of Antimalarial Activity

Megan Okada[a], Ping Guo[a], Shai-anne Nalder[a], and Paul A. Sigala[a,1]

[a]Department of Biochemistry, University of Utah School of Medicine, Salt Lake City, UT 84112

[1]To whom correspondence may be addressed: p.sigala@biochem.utah.edu

ORCID ID:
(M.O.) 0000-0003-4398-9819
(P.G.) 0000-0003-3023-779X
(S.N.) 0000-0002-6892-9321
(P.A.S.) 0000-0002-3464-3042

Author contributions: P.A.S. designed research; P.G., S.N., M.O., and P.A.S. performed research and analyzed data; P.A.S. wrote the paper.

The authors declare no competing interests.

Abstract: Doxycycline (DOX) is a key antimalarial drug thought to kill *Plasmodium* parasites by blocking protein translation in the essential apicoplast organelle. Clinical use is primarily limited to prophylaxis due to delayed second-cycle parasite death at 1-3 μM serum concentrations. DOX concentrations >5 μM kill parasites with first-cycle activity but have been ascribed to off-target mechanisms outside the apicoplast. We report that 10 μM DOX blocks apicoplast biogenesis in the first cycle and is rescued by isopentenyl pyrophosphate, an essential apicoplast product, confirming an apicoplast-specific mechanism. Exogenous iron rescues parasites and apicoplast biogenesis from first- but not second-cycle effects of 10 μM DOX, revealing that first-cycle activity involves a metal-dependent mechanism distinct from the delayed-death mechanism. These results critically expand the paradigm for understanding the fundamental antiparasitic mechanisms of DOX and suggest repurposing DOX as a faster-acting antimalarial at higher dosing whose multiple mechanisms would be expected to limit parasite resistance.

INTRODUCTION

Malaria remains a serious global health problem, with hundreds of thousands of annual deaths due to *Plasmodium falciparum* parasites. The absence of a potent, long-lasting vaccine and parasite tolerance to frontline artemisinin combination therapies continue to challenge malaria elimination efforts. Furthermore, there are strong concerns that the current COVID-19 pandemic will disrupt malaria prevention and treatment efforts in Africa and cause a surge in malaria deaths that unravels decades of progress (1). Deeper understanding of basic parasite biology and the mechanisms of current drugs will guide their optimal use for malaria prevention and treatment and facilitate development of novel therapies to combat parasite drug resistance.

Tetracycline antibiotics like DOX are thought to kill eukaryotic *P. falciparum* parasites by inhibiting prokaryotic-like 70S ribosomal translation inside the essential apicoplast organelle (Figure 1) (2). Although stable *P. falciparum* resistance to DOX has not been reported, clinical use is largely limited to prophylaxis due to delayed activity against intraerythrocytic infection (3, 4). Parasites treated with 1-3 μM DOX, the drug concentration sustained in human serum with current 100-200 mg dosage (5), continue to grow for 72-96 hours and only die after the second 48-hour intraerythrocytic growth cycle when they fail to expand into a third cycle (2). Slow antiparasitic activity is believed to be a fundamental limitation of DOX and other antibiotics that block apicoplast-maintenance pathways (4, 6). First-cycle anti-*Plasmodium* activity has been reported for DOX and azithromycin concentrations >3 μM, but such activities have been ascribed to targets outside the apicoplast (2, 7, 8). A more incisive understanding of the mechanisms and parameters that govern first versus second-cycle DOX activity can inform and improve clinical use of this valuable antibiotic for antimalarial treatment. We therefore set out to test and unravel the mechanisms and apicoplast specificity of first-cycle DOX activity.

RESULTS AND DISCUSSION

First-cycle activity by 10 µM DOX has an apicoplast-specific mechanism. Prior studies have shown that 200 µM isopentenyl pyrophosphate (IPP), an essential apicoplast product, rescues parasites from the delayed-death activity of 1-3 µM DOX, confirming an apicoplast-specific target (7). To provide a baseline for comparison, we first used continuous-growth and 48-hour growth-inhibition assays to confirm that IPP rescued parasites from 1 µM DOX (Figure 2A) and that DOX concentrations >5 µM killed parasites with first-cycle activity (Figure 2A – C and Figure 2- figure supplement 1) as previously reported (2). To test the apicoplast specificity of first-cycle DOX activity, we next asked whether 200 µM IPP could rescue parasites from DOX concentrations >5 µM. We observed that IPP shifted the 48-hour EC_{50} value of DOX from 5 ± 1 to 12 ± 2 µM (average ± SD of 5 independent assays, P = 0.001 by unpaired t-test) (Figure 2C and Figure 2-figure supplement 1), suggesting that first-cycle growth defects from 5-10 µM DOX reflect an apicoplast-specific mechanism but that DOX concentrations >10 µM cause off-target defects outside this organelle. We further tested this conclusion using continuous growth assays performed at constant DOX concentrations. We observed that IPP fully or nearly fully rescued parasites from first-cycle growth inhibition by 10 µM but not 20 or 40 µM Dox (Figure 2A & 2D and Figure 2-figure supplement 1). On the basis of IPP rescue, we conclude that 10 µM DOX kills *P. falciparum* with first-cycle activity by an apicoplast-specific mechanism.

10 µM DOX blocks apicoplast biogenesis in the first cycle: Inhibition of apicoplast biogenesis in the second intraerythrocytic cycle is a hallmark of 1-3 µM DOX-treated *P. falciparum*, resulting in unviable parasite progeny that fail to inherit the organelle (2). IPP rescues parasite viability after the second cycle without rescuing apicoplast inheritance, such that third-cycle daughter parasites

lack the organelle and accumulate apicoplast-targeted proteins in cytoplasmic vesicles (7). We treated synchronized ring-stage D10 (9) or NF54 (10) parasites expressing the acyl carrier protein leader sequence fused to GFP (ACP_L-GFP) with 10 μM DOX and assessed apicoplast morphology 30-36 hours later in first-cycle schizonts. In contrast to the second-cycle effects of 1-3 μM DOX, the apicoplast in 10 μM DOX-treated parasites failed to elongate in the first cycle. Rescue by 200 μM IPP produced second-cycle parasite progeny with a dispersed GFP signal indicative of apicoplast loss (Figure 2E and Figure 2- figure supplement 2). We conclude that 10 μM DOX blocks apicoplast biogenesis in the first cycle.

First- and second-cycle effects of DOX on the apicoplast are due to distinct mechanisms. What is the molecular mechanism of faster apicoplast-specific activity by 10 μM DOX? We first considered the model that both 1 and 10 μM DOX inhibit apicoplast translation but that 10 μM DOX kills parasites faster due to more stringent translation inhibition at higher drug concentrations. This model predicts that treating parasites simultaneously with multiple distinct apicoplast-translation inhibitors, each added at a delayed death-inducing concentration, will produce additive, accelerated activity that kills parasites in the first cycle. To test this model, we treated synchronized D10 parasites with combinatorial doses of 2 μM DOX, 2 μM clindamycin, and 500 nM azithromycin and monitored growth over 3 intraerythrocytic cycles. Treatment with each antibiotic alone produced major growth defects at the end of the second cycle, as expected for delayed-death activity at these concentrations (6). Two- and three-way drug combinations caused growth defects that were indistinguishable from individual treatments and provided no evidence for additive, first-cycle activity (Figure 3A and Figure 3- figure supplement 1). These

results contradict a simple model that 1 and 10 µM DOX act via a common translation-blocking mechanism and suggest that the first-cycle activity of 10 µM DOX is due to a distinct mechanism.

Exogenous iron rescues parasites from first- but not second-cycle effects of 10 µM DOX. Tetracycline antibiotics like DOX tightly chelate a wide variety of di- and trivalent metal ions via their siderophore-like arrangement of exocyclic hydroxyl and carbonyl groups (Figure 1), with a reported affinity series of Fe^{3+}>Fe^{2+}>Zn^{2+}>Mg^{2+}>Ca^{2+} (11, 12). Indeed, tetracycline interactions with Ca^{2+} and Mg^{2+} ions mediate cellular uptake and binding to biomolecular targets such as the tetracycline repressor and 16S rRNA (12, 13). We next considered a model that first-cycle effects of 10 µM DOX reflect a metal-dependent mechanism distinct from ribosomal inhibition causing second-cycle death. To test this model, we investigated whether exogenous metals rescued parasites from 10 µM DOX. We failed to observe growth rescue by 10 µM $ZnCl_2$ (toxicity limit (14)) or 500 µM $CaCl_2$ in continuous-growth (Figure 3B and Figure 3- figure supplement 1) or 48-hour growth-inhibition assays (Figure 3C). In contrast, 500 µM $FeCl_3$ (and to a lesser extent 500 µM $MgCl_2$) fully or nearly fully rescued parasites from first-cycle growth inhibition by 10 µM DOX (Figure 3C & 3D), although partial rescue was observed at $FeCl_3$ concentrations as low as 50 µM (Figure 3- figure supplement 1). However, parasites treated with 10 µM DOX and 500 µM $FeCl_3$ still succumbed to second-cycle, delayed death (Figure 3D and Figure 3- figure supplement 1), as expected for distinct mechanisms of first- and second-cycle DOX activity.

We also observed that 500 µM $FeCl_3$ but not $CaCl_2$ rescued first-cycle apicoplast-branching in 10 µM DOX (Figure 3E and Figure 3- figure supplement 2). These observations contrast with IPP, which rescued parasite viability in 10 µM DOX but did not restore apicoplast branching (Figure 2E). We further noted that $FeCl_3$ selectively rescued parasites from the

apicoplast-specific, first-cycle growth effects of 10 µM DOX but did not rescue parasites from the second-cycle effects of 1 µM DOX (Figures 3F) or the off-target effects of 20-40 µM DOX (Figure 3G and Figure 3- figure supplement 1). We conclude that 10 µM DOX kills parasites via a metal-dependent, first-cycle mechanism that blocks apicoplast biogenesis and is distinct from the second-cycle, delayed-death mechanism of 1 µM DOX.

Metal-dependent mechanisms of first-cycle activity by 10 µM DOX. What is the metal-dependent mechanism of 10 µM DOX, and why is there preferential rescue by $FeCl_3$? Tetracyclines bind iron more tightly than other metals, with an equilibrium association constant of 10^{10} M^{-1} for 1:1 chelation of Fe^{3+} versus 10^4 M^{-1} for Mg^{2+} (11). Although the 500 µM concentration of exogenous $FeCl_3$ required for maximal rescue of parasite growth in 10 µM DOX is large relative to the ~1 µM labile iron concentration estimated for the parasite cytoplasm (15), the intracellular iron concentration achieved by exogenous addition of 500 µM $FeCl_3$ remains unclear. Indeed, mechanisms of iron uptake and trafficking by blood-stage *P. falciparum* remain sparsely understood (15, 16), especially uptake across the four membranes that surround the apicoplast.

We first considered whether exogenous $FeCl_3$ might selectively rescue 10 µM DOX activity by blocking or reducing its uptake into the parasite apicoplast, since metal chelation has been reported to influence the cellular uptake of tetracycline antibiotics in other organisms (12). However, 500 µM $FeCl_3$ or $MgCl_2$ did not rescue second-cycle parasite death in continuous growth assays with 10 µM (Figures 3D) or 1 µM DOX (Figure 3F). Furthermore, exogenous iron resulted in only a small, 1.5-µM shift in EC_{50} value from 0.5 to 2 µM in a 96-hour growth inhibition assay, in contrast to the 10.5-µM shift provided by IPP (Figure 3- figure supplement 1). These results strongly suggest that DOX uptake into the apicoplast is not substantially perturbed by exogenous

iron. The inability of 500 μM $FeCl_3$ to rescue first-cycle activity by ≥20-μM DOX (Figure 3G) further suggests that general uptake of DOX into parasites is not substantially affected by exogenous iron.

We propose two distinct models to explain the metal-dependent effects of 10 μM DOX, both of which could contribute to apicoplast-specific activity. First, DOX could directly bind and sequester labile iron within the apicoplast, reducing its bioavailability for Fe-S cluster biogenesis and other essential iron-dependent processes in this organelle. Indeed, prior work has shown that apicoplast biogenesis requires Fe-S cluster synthesis apart from known essential roles in isoprenoid biosynthesis (17). In this first model, rescue by exogenous $FeCl_3$ would be due to restoration of iron bioavailability, while modest rescue by 500 μM $MgCl_2$ may reflect competitive displacement of DOX-bound iron to restore iron bioavailability. RPMI growth medium already contains ~400 μM Mg^{2+} prior to supplementation with an addition 500 μM $MgCl_2$, and thus Mg^{2+} availability is unlikely to be directly limited by 10 μM DOX. Consistent with a general mechanism that labile-iron chelation can block apicoplast biogenesis, we observed in preliminary studies that the anti-*Plasmodium* growth inhibition caused by the highly-specific iron chelator, deferoxamine (DFO) (16), could be partially rescued by IPP, fully rescued by exogenous $FeCl_3$, and involved a first-cycle defect in apicoplast branching/division (Figure 3- figure supplement 3). Development of targeted and incisive probes of labile iron within subcellular compartments remains an ongoing challenge in biology (18), especially in the *Plasmodium* apicoplast where iron uptake, concentration, and utilization remain sparsely understood. To evaluate the impact of DOX on iron availability in the apicoplast, we are developing protein-based probes of lipoic acid and isoprenoid biosynthesis, as these two apicoplast-dependent processes require Fe/S-cluster biosynthesis for activity (17).

In a second model, DOX could bind to additional macromolecular targets within the apicoplast (e.g., a metalloenzyme) via metal-dependent interactions that inhibit essential functions required for organelle biogenesis. Exogenous 500 μM Fe^{3+} would then rescue parasites by disrupting these inhibitory interactions via competitive binding to DOX. This second model would be mechanistically akin to diketo acid inhibitors of HIV integrase like raltegravir that bind to active site Mg^{2+} ions to inhibit integrase activity but are displaced by exogenous metals (19, 20). To test this model, we are developing a DOX-affinity reagent to identify apicoplast targets that interact with doxycycline and whose inhibition may contribute to first-cycle DOX activity.

Conclusions and implications. These results critically expand the paradigm for understanding the fundamental mechanisms of DOX activity against *P. falciparum* malaria parasites. These mechanisms include a delayed, second-cycle defect at 1-3 μM DOX that likely reflects inhibition of 70S apicoplast ribosomes, a first-cycle iron-dependent defect within the apicoplast that uniquely operates at 8-10 μM DOX, and a first-cycle iron-independent mechanism outside the apicoplast at ≥20 μM DOX (Figure 1). Pharmacokinetic studies indicate that current 100-200 mg doses of DOX achieve peak human serum concentrations of 6-8 μM over the first six hours which then decrease to 1-2 μM over 24 hours (5). Although current DOX treatment regimens result in delayed parasite clearance in vivo, both apicoplast-specific mechanisms of DOX likely operate over this concentration range and contribute to parasite death (2). These multiple mechanisms of DOX, together with limited antimalarial use of DOX in the field, may explain why parasites with stable DOX resistance have not emerged (3, 4).

There has been a prevailing view in the literature that delayed-death activity is a fundamental limitation of antibiotics like DOX that block apicoplast maintenance (21, 22). Our

results emphasize that DOX is not an intrinsically slow-acting antimalarial drug and support the emerging paradigm (23-25) that inhibition of apicoplast biogenesis can defy the delayed-death phenotype to kill parasites on a faster time-scale. The first-cycle, iron-dependent impacts of 10 μM DOX or 15 μM DFO on apicoplast biogenesis also suggest that this organelle may be especially susceptible to therapeutic strategies that interfere with acquisition and utilization of iron, perhaps due to limited uptake of exogenous iron and/or limited iron storage mechanisms in the apicoplast.

Finally, this work suggests the possibility of repurposing DOX as a faster-acting antiparasitic treatment at higher dosing, whose multiple mechanisms would be expected to limit parasite resistance. Prior studies indicate that 500-600 mg doses in humans achieve sustained serum DOX concentrations ≥5 μM for 24-48 hours with little or no increase in adverse effects (26, 27). DOX is currently contraindicated for long-term prophylaxis in pregnant women and young children, two of the major at-risk populations for malaria, due to concerns about impacts on fetal development and infant tooth discoloration, respectively, based on observed toxicities for other tetracyclines (28). Recent studies suggest that these effects are not associated with short-term DOX use (28, 29), but more work is needed to define the safety parameters that would govern short-term use of DOX for treatment in these populations. Recent development of tetracycline derivatives with improved activities may provide another option to deploy this important class of antibiotics for antimalarial treatment (30).

METHODS

Materials: All reagents were cell-culture grade and/or of the highest purity commercially available. The vendor and catalog number are given for individual compounds when first mentioned.

Parasite culture: All experiments were performed using *Plasmodium falciparum* Dd2, ACP_L-GFP D10 (9), or ACP_L-GFP NF54 (10) parasite strains. Parasite culturing was performed as previously described (31) in Roswell Park Memorial Institute medium (RPMI-1640, Thermo Fisher 23400021) supplemented with 2.5 g/L Albumax I Lipid-Rich BSA (Thermo Fisher 11020039), 15 mg/L hypoxanthine (Sigma H9636), 110 mg/L sodium pyruvate (Sigma P5280), 1.19 g/L HEPES (Sigma H4034), 2.52 g/L sodium bicarbonate (Sigma S5761), 2 g/L glucose (Sigma G7021), and 10 mg/L gentamicin (Invitrogen Life Technologies 15750060). Cultures were maintained at 2% hematocrit in human erythrocytes obtained from the University of Utah Hospital blood bank, at 37 ˚C, and at 5% O_2, 5% CO_2, 90% N_2.

Parasite Growth Assays: Parasites were synchronized to the ring stage either by treatment with 5% D-sorbitol (Sigma S7900) or by first magnet-purifying schizonts and then incubating them with uninfected erythrocytes for five hours followed by treatment with 5% D-sorbitol. Results from growth assays using either of these synchronization methods were indistinguishable, and 5% sorbitol was used for synchronization unless stated otherwise. For continuous growth assays, parasite growth was monitored by diluting sorbitol-synchronized parasites to ~0.5% starting parasitemia, adding additional treatments (antibiotics, IPP, and/or metal salts) at assay initiation, and allowing culture expansion over several days with daily media changes. Growth assays with

doxycycline (Sigma D3447), clindamycin (Sigma C6427), and azithromycin (Sigma 75199) were conducted at 0.2% DMSO at the indicated final drug concentration. Growth assays with $ZnCl_2$ (Sigma 208086), $CaCl_2$ (Sigma C4901), $MgCl_2$ (M8266), $FeCl_3$ (Sigma 236489), deferoxamine (Sigma D9533), and/or IPP (NH_4^+ salt, Isoprenoids IPP001) were conducted at the indicated final concentrations. Parasitemia was monitored daily by flow cytometry by diluting 10 µl of each parasite culture well from 2-3 biological replicates into 200µl of 1.0 µg/ml acridine orange (Invitrogen Life Technologies A3568) in phosphate buffered saline (PBS) and analysis on a BD FACSCelesta system monitoring SSC-A, FSC-A, PE-A, FITC-A, and PerCP-Cy5-5-A channels. For EC_{50} determinations via dose-response assay, synchronous ring-stage parasites were diluted to 1% parasitemia and incubated with variable (serially two-fold diluted) DOX concentrations ±200 µM IPP, ±50 µM mevalonate (Cayman 20348), ±500 µM $FeCl_3$, or ±500 µM $CaCl_2$ for 48-120 hours without media changes. Parasitemia was determined by flow cytometry for 2-4 biological replicates for each untreated or drug-treated condition, normalized to the parasitemia in the absence of drug, plotted as the average ±SD of biological replicates as a function of the log of the drug concentration (in µM), and fit to a 4-parameter dose-response model using GraphPad Prism 8.0. All growth assays were independently repeated 2-4 times on different weeks and in different batches of blood. The 48-hour EC_{50} values determined from five independent assays for DOX ±IPP were averaged and analyzed by unpaired t-test using GraphPad Prism 8.0.

Fluorescence Microscopy: For live-cell experiments, parasites samples were collected at 30-36 or 65 hours after synchronization with magnet purification plus sorbitol treatment (see above). Imaging experiments were independently repeated twice. Parasite nuclei were visualized by incubating samples with 1-2 µg/ml Hoechst 33342 (Thermo Scientific Pierce 62249) for 10-20

minutes at room temperature. The parasite apicoplast was visualized in D10 (9) or NF54 mevalonate-bypass (10) cells using the ACP_{leader}-GFP expressed by both lines. Images were taken on DIC/brightfield, DAPI, and GFP channels using either a Zeiss Axio Imager or an EVOS M5000 imaging system. Fiji/ImageJ was used to process and analyze images. All image adjustments, including contrast and brightness, were made on a linear scale. For indicated conditions, apicoplast morphologies in 20-40 parasites were scored as elongated, focal, or dispersed; counted; and plotted by histogram as the fractional population with the indicated morphology. Analysis of replicate samples indicated standard deviations that were <10% for all samples in the percentage of parasites displaying a given apicoplast morphology in a given condition. Unpaired t-test analysis using GraphPad Prism was used to evaluate the significance of observed population differences.

ACKNOWLEDGEMENTS. We thank Jeremy Burrows, Dan Goldberg, Don Granger, Daria Hazuda, Jerry Kaplan, Sean Prigge, Dennis Winge and members of the Sigala lab for helpful discussions. P.A.S. holds a Career Award at the Scientific Interface from the Burroughs Wellcome Fund and a Pew Biomedical Scholarship from the Pew Charitable Trusts. Microscopy and flow cytometry were performed using core facilities at the University of Utah.

References:

1. Weiss DJ, *et al.* (2020) Indirect effects of the COVID-19 pandemic on malaria intervention coverage, morbidity, and mortality in Africa: a geospatial modelling analysis. *Lancet Infect. Dis.* http://dx.doi.org/10.1016/S1473-3099(20)30700-3.
2. Dahl EL, *et al.* (2006) Tetracyclines specifically target the apicoplast of the malaria parasite Plasmodium falciparum. *Antimicrob. Agents Chemother.* 50(9):3124-3131. http://dx.doi.org/10.1128/AAC.00394-06.
3. Conrad MD & Rosenthal PJ (2019) Antimalarial drug resistance in Africa: the calm before the storm? *Lancet Infect. Dis.* 19(10):e338-e351. http://dx.doi.org/10.1016/S1473-3099(19)30261-0.

4. Gaillard T, Madamet M, & Pradines B (2015) Tetracyclines in malaria. *Malar. J.* 14:445. http://dx.doi.org/10.1186/s12936-015-0980-0.
5. Newton PN, *et al.* (2005) Pharmacokinetics of oral doxycycline during combination treatment of severe falciparum malaria. *Antimicrob. Agents Chemother.* 49(4):1622-1625. http://dx.doi.org/10.1128/AAC.49.4.1622-1625.2005.
6. Dahl EL & Rosenthal PJ (2007) Multiple antibiotics exert delayed effects against the Plasmodium falciparum apicoplast. *Antimicrob. Agents Chemother.* 51(10):3485-3490. http://dx.doi.org/10.1128/AAC.00527-07.
7. Yeh E & DeRisi JL (2011) Chemical rescue of malaria parasites lacking an apicoplast defines organelle function in blood-stage Plasmodium falciparum. *PLoS Biol.* 9(8):e1001138. http://dx.doi.org/10.1371/journal.pbio.1001138.
8. Wilson DW, *et al.* (2015) Macrolides rapidly inhibit red blood cell invasion by the human malaria parasite, Plasmodium falciparum. *BMC Biol.* 13:52. http://dx.doi.org/10.1186/s12915-015-0162-0.
9. Waller RF, Reed MB, Cowman AF, & McFadden GI (2000) Protein trafficking to the plastid of *Plasmodium falciparum* is via the secretory pathway. *EMBO J.* 19(8):1794-1802. http://dx.doi.org/10.1093/emboj/19.8.1794.
10. Swift RP, *et al.* (2020) A mevalonate bypass system facilitates elucidation of plastid biology in malaria parasites. *PLoS Pathog.* 16(2):e1008316. http://dx.doi.org/10.1371/journal.ppat.1008316.
11. Albert A & Rees CW (1956) Avidity of the tetracyclines for the cations of metals. *Nature* 177(4505):433-434. http://dx.doi.org/10.1038/177433a0.
12. Nelson ML (1998) Chemical and biological dynamics of tetracyclines. *Adv. Dent. Res.* 12(2):5-11. http://dx.doi.org/10.1177/08959374980120011901.
13. Orth P, Schnappinger D, Hillen W, Saenger W, & Hinrichs W (2000) Structural basis of gene regulation by the tetracycline inducible Tet repressor-operator system. *Nat. Struct. Biol.* 7(3):215-219. http://dx.doi.org/10.1038/73324.
14. Marvin RG, *et al.* (2012) Fluxes in "free" and total zinc are essential for progression of intraerythrocytic stages of Plasmodium falciparum. *Chem. Biol.* 19(6):731-741. http://dx.doi.org/10.1016/j.chembiol.2012.04.013.
15. Scholl PF, Tripathi AK, & Sullivan DJ (2005) Bioavailable iron and heme metabolism in *Plasmodium falciparum*. *Curr. Top. Microbiol. Immunol.* 295:293-324.
16. Mabeza GF, Loyevsky M, Gordeuk VR, & Weiss G (1999) Iron chelation therapy for malaria: a review. *Pharmacol. Ther.* 81(1):53-75. http://dx.doi.org/10.1016/s0163-7258(98)00037-0.
17. Gisselberg JE, Dellibovi-Ragheb TA, Matthews KA, Bosch G, & Prigge ST (2013) The suf iron-sulfur cluster synthesis pathway is required for apicoplast maintenance in malaria parasites. *PLoS Path.* 9(9):e1003655. http://dx.doi.org/10.1371/journal.ppat.1003655.
18. Breuer W, Shvartsman M, & Cabantchik ZI (2008) Intracellular labile iron. *Int. J. Biochem. Cell Biol.* 40(3):350-354. http://dx.doi.org/10.1016/j.biocel.2007.03.010.
19. Grobler JA, *et al.* (2002) Diketo acid inhibitor mechanism and HIV-1 integrase: implications for metal binding in the active site of phosphotransferase enzymes. *Proc. Natl. Acad. Sci. U.S.A.* 99(10):6661-6666. http://dx.doi.org/10.1073/pnas.092056199.
20. Hare S, Gupta SS, Valkov E, Engelman A, & Cherepanov P (2010) Retroviral intasome assembly and inhibition of DNA strand transfer. *Nature* 464(7286):232-236. http://dx.doi.org/10.1038/nature08784.

21. Ramya TN, Mishra S, Karmodiya K, Surolia N, & Surolia A (2007) Inhibitors of nonhousekeeping functions of the apicoplast defy delayed death in Plasmodium falciparum. *Antimicrob. Agents Chemother.* 51(1):307-316. http://dx.doi.org/10.1128/AAC.00808-06.
22. Kennedy K, Crisafulli EM, & Ralph SA (2019) Delayed Death by Plastid Inhibition in Apicomplexan Parasites. *Trends Parasitol* 35(10):747-759. http://dx.doi.org/10.1016/j.pt.2019.07.010.
23. Boucher MJ & Yeh E (2019) Disruption of Apicoplast Biogenesis by Chemical Stabilization of an Imported Protein Evades the Delayed-Death Phenotype in Malaria Parasites. *mSphere* 4(1). http://dx.doi.org/10.1128/mSphere.00710-18.
24. Amberg-Johnson K*, et al.* (2017) Small molecule inhibition of apicomplexan FtsH1 disrupts plastid biogenesis in human pathogens. *eLife* 6. http://dx.doi.org/10.7554/eLife.29865.
25. Uddin T, McFadden GI, & Goodman CD (2018) Validation of Putative Apicoplast-Targeting Drugs Using a Chemical Supplementation Assay in Cultured Human Malaria Parasites. *Antimicrob. Agents Chemother.* 62(1). http://dx.doi.org/10.1128/AAC.01161-17.
26. Marlin GE & Cheng S (1979) Pharmacokinetics and tolerability of a single oral 600-mg dose of doxycycline. *Med. J. Aust.* 1(12):575-576. http://dx.doi.org/10.5694/j.1326-5377.1979.tb142053.x.
27. Adadevoh BK, Ogunnaike IA, & Bolodeoku JO (1976) Serum levels of doxycycline in normal subjects after a single oral dose. *Br. Med. J.* 1(6014):880. http://dx.doi.org/10.1136/bmj.1.6014.880.
28. Gaillard T, Boxberger M, Madamet M, & Pradines B (2018) Has doxycycline, in combination with anti-malarial drugs, a role to play in intermittent preventive treatment of Plasmodium falciparum malaria infection in pregnant women in Africa? *Malar. J.* 17(1):469. http://dx.doi.org/10.1186/s12936-018-2621-x.
29. Todd SR*, et al.* (2015) No visible dental staining in children treated with doxycycline for suspected Rocky Mountain Spotted Fever. *J Pediatr* 166(5):1246-1251. http://dx.doi.org/10.1016/j.jpeds.2015.02.015.
30. Draper MP*, et al.* (2013) In vitro and in vivo antimalarial efficacies of optimized tetracyclines. *Antimicrob. Agents Chemother.* 57(7):3131-3136. http://dx.doi.org/10.1128/AAC.00451-13.
31. Sigala PA, Crowley JR, Henderson JP, & Goldberg DE (2015) Deconvoluting heme biosynthesis to target blood-stage malaria parasites. *eLife* 4. http://dx.doi.org/10.7554/eLife.09143.

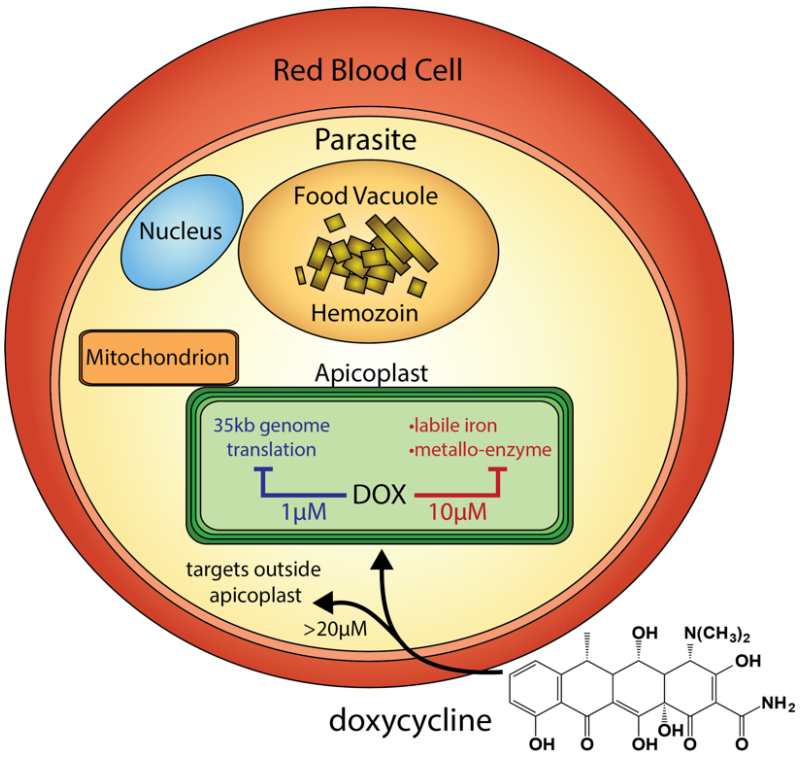

Figure 1. Scheme of intraerythrocytic *P. falciparum* parasite depicting doxycycline, its canonical delayed-death mechanism at 1 µM inhibiting apicoplast genome translation, the novel metal-dependent mechanism(s) in the apicoplast explored herein at 10 µM, and off-target activity outside the apicoplast at >20 µM.

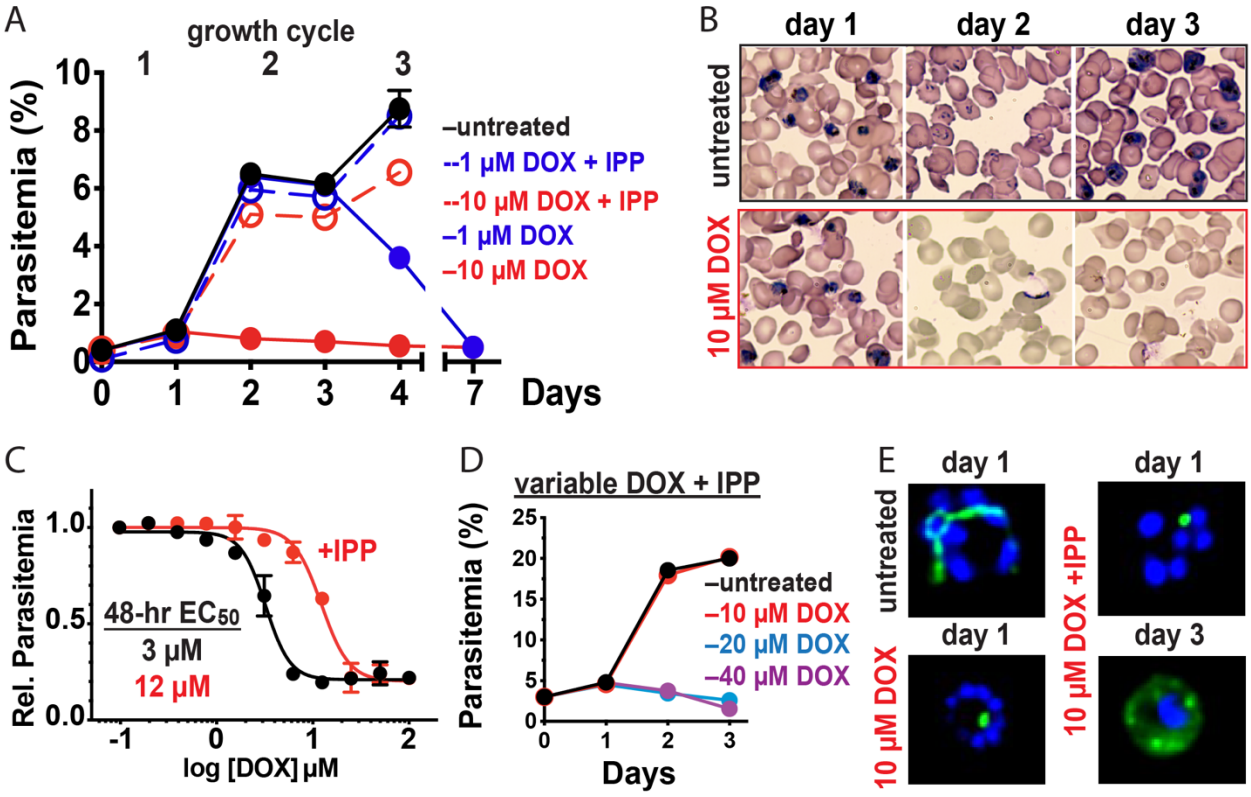

Figure 2. 10 µM doxycycline kills *P. falciparum* with first-cycle, apicoplast-specific activity. (A) Continuous growth assay of synchronized Dd2 parasites treated with 1 or 10 µM DOX ±200 µM IPP with (B) Giemsa-stained blood smears for days 1-3. (C) 48-hour growth-inhibition curve for DOX-treated Dd2 parasites ±200 µM IPP. (D) Continuous growth assay of synchronized Dd2 parasites treated with 10 – 40 µM DOX and 200 µM IPP. (E) Epifluorescence images of synchronized parasites treated as rings with 10 µM DOX ±200 µM IPP and imaged 36 or 65 hours later (green = ACP_L-GFP, blue = nuclear Hoechst stain). Data points in growth assays are the average ±SD of biological replicates. All growth assays were independently repeated 2 – 4 times using different batches of blood (shown in Figure 2- figure supplement 1).

The following figure supplements are available for figure 2:

Figure supplement 1. Additional, independent growth assays with DOX and IPP.

Figure supplement 2. Additional epifluorescence images of DOX-treated parasites and analysis.

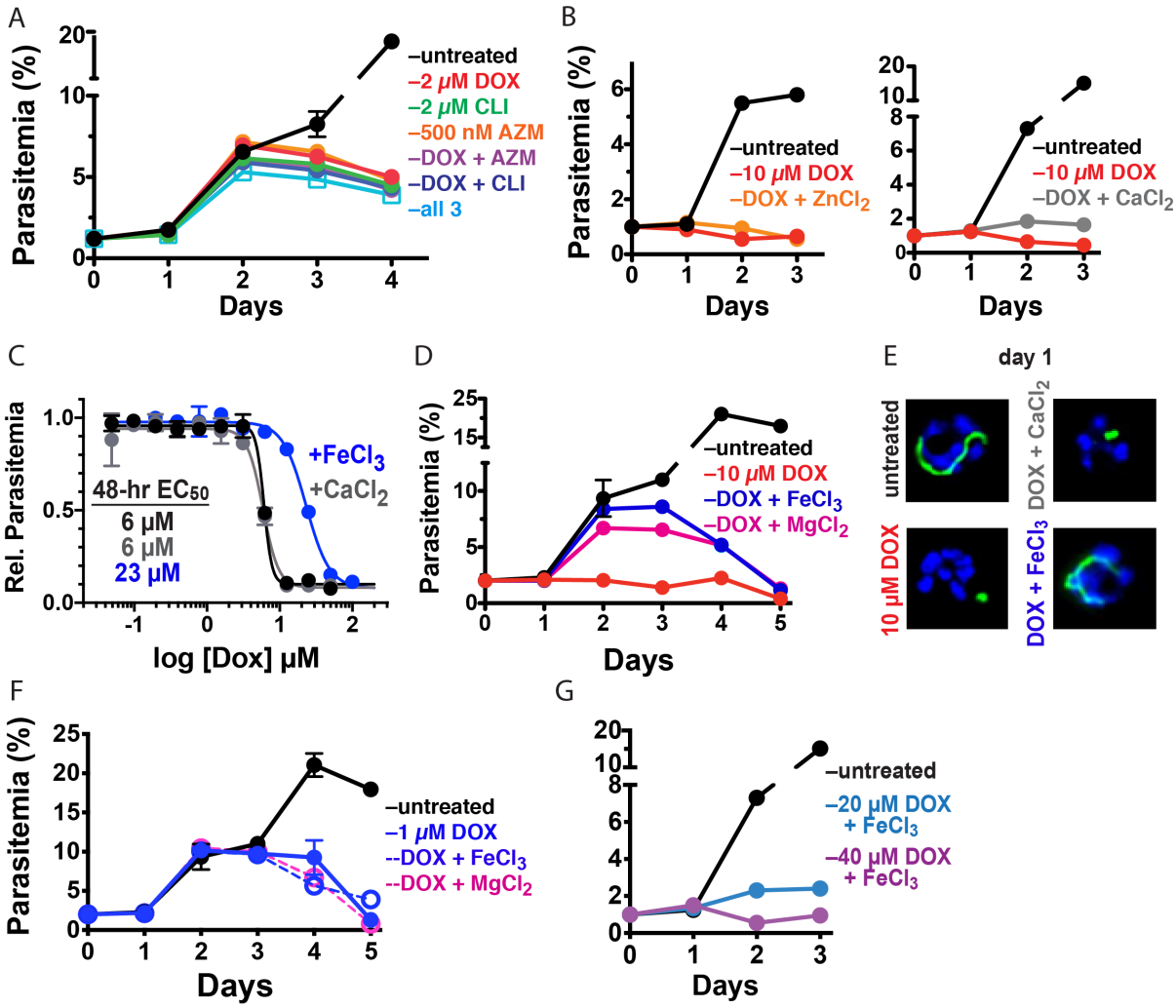

Figure 3. 10 μM DOX kills *P. falciparum* with a first-cycle, metal-dependent mechanism. Continuous growth assays of synchronized Dd2 parasites treated with (A) DOX, clindamycin (CLI), and/or azithromycin (AZM) and (B) 10 μM DOX and 10 μM $ZnCl_2$ or 500 μM $CaCl_2$. (C) 48-hour growth inhibition assay of D10 parasites treated with DOX without or with 500 μM $FeCl_3$ or $CaCl_2$. (D) Continuous growth assay of synchronized Dd2 parasites treated with 10 μM DOX and 500 μM $FeCl_3$ or $MgCl_2$. (E) Epifluorescence images of synchronized parasites treated as rings with 10 μM DOX ±500 μM $FeCl_3$ or $CaCl_2$ and imaged 36 hours later (green = ACP_L-GFP, blue = nuclear Hoechst stain). (F) Continuous growth assay of synchronized Dd2 parasites treated with 1 μM DOX and 500 μM $FeCl_3$ or $MgCl_2$. (G) Continuous-growth assay of synchronized Dd2 parasites treated with 20 or 40 μM DOX and 500 μM $FeCl_3$. Data points in growth assays are the average ±SD of biological replicates. All growth assays were independently repeated using different batches of blood (shown in Figure 3- figure supplement 1).

The following figure supplements are available for figure 3:

Figure supplement 1. Additional independent growth assays with DOX, antibiotics, and metals.

Figure supplement 2. Additional images and analysis of parasites treated with DOX and metals.

Figure supplement 3. Effect of deferoxamine on parasite growth and apicoplast biogenesis.

Supplemental Figures

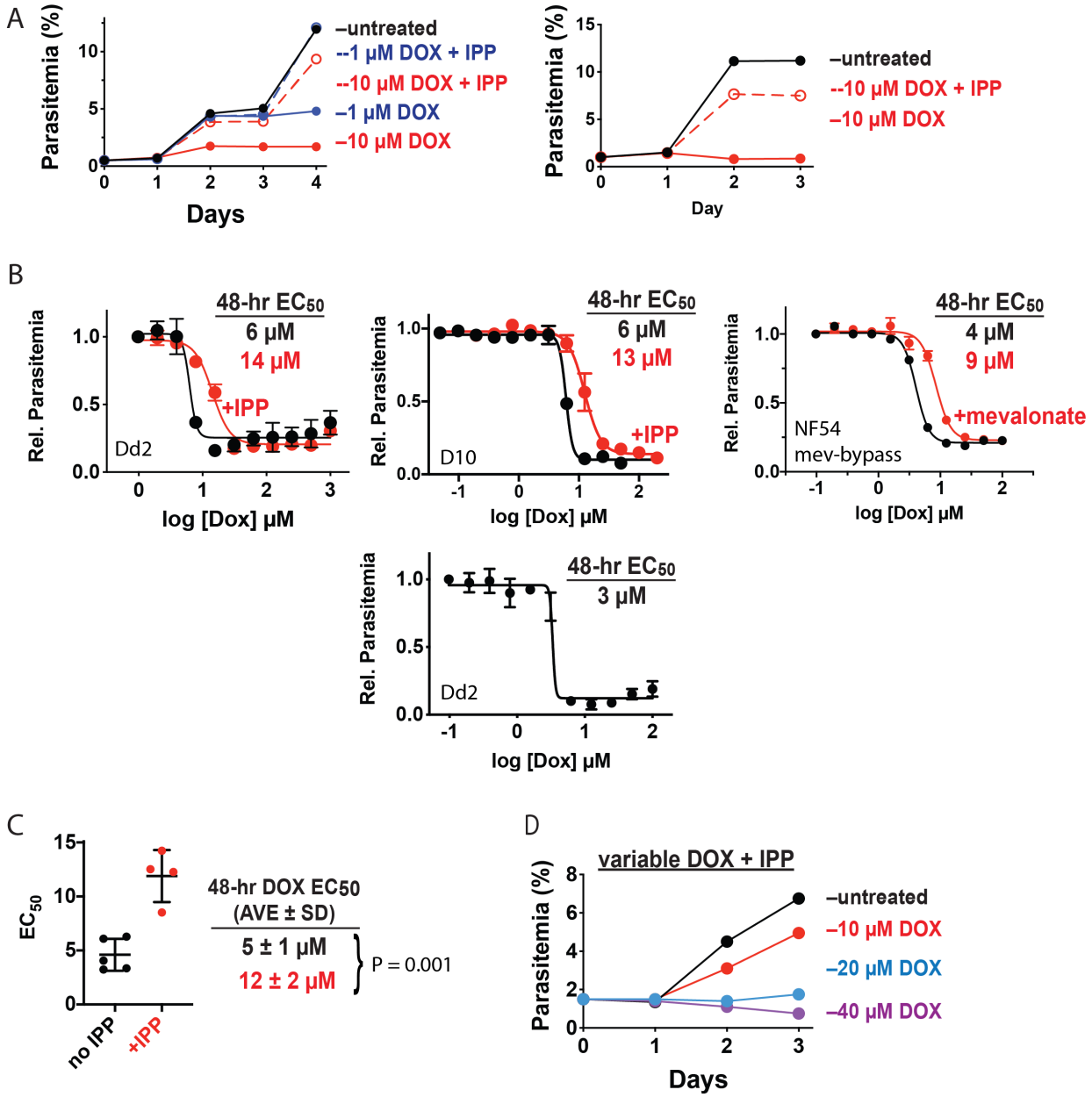

Figure 2- figure supplement 1. Additional, independent growth assays with DOX and IPP. (A) Additional continuous growth assays of synchronized Dd2 parasites treated with 1 or 10 µM DOX ±200 µM IPP. (B) Independent 48-hour growth-inhibition assays for DOX-treated Dd2, D10, NF54 parasites in the absence or presence of 200 µM IPP or 50 µM mevalonate. Dd2 and NF54 parasites were synchronized by single treatment with 5% D-sorbitol. D10 parasites were synchronized by magnet purification of schizonts followed by 5-hour incubation with uninfected erythrocytes and treatment with 5% D-sorbitol. Data points in individual plots are the ave ±sd of 2-4 biological replicates. Each plot reflects an independent assay performed with a different batch of blood. (C) Scatter plot of doxycycline EC_{50} values from independent assays ±IPP with calculated ave ± sd and analysis by unpaired t-test. (D) Independent continuous growth assay of synchronized Dd2 parasites treated with 10 – 40 µM DOX and 200 µM IPP.

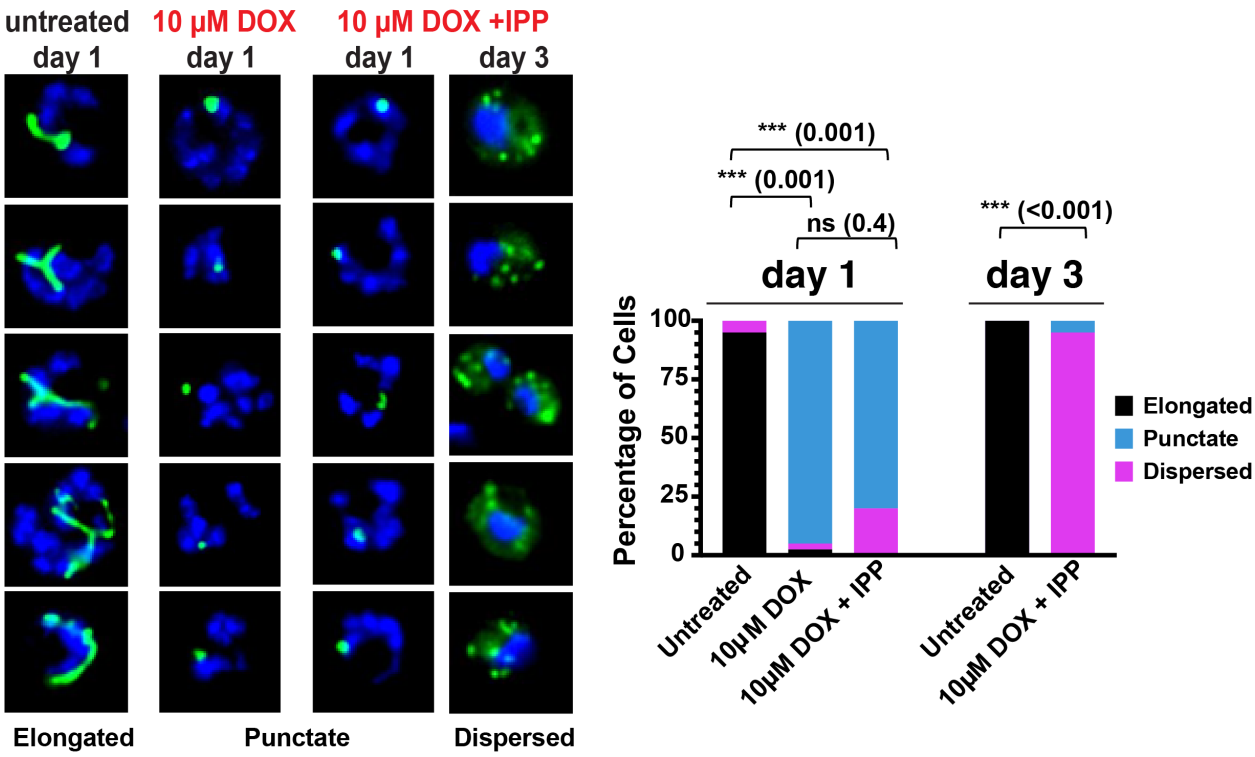

Figure 2- figure supplement 2. Additional epifluorescence images of DOX-treated D10 parasites. Magnet plus sorbitol-synchronized parasites were treated as rings with 10 µM DOX ±200 µM IPP and imaged 1 or 3 days later (green = ACP_L-GFP, blue = nuclear Hoechst stain). 20-40 parasites were examined for each treatment condition on each given day for duplicate experiments, and data were plotted as the average percentage of parasites in each population that displayed an elongated, punctate, or dispersed apicoplast GFP signal. For clarity, error bars are not displayed but standard deviations were <10% in all conditions. Cell-percentage differences were analyzed by unpaired t-test (P values in parentheses, ns = not significant).

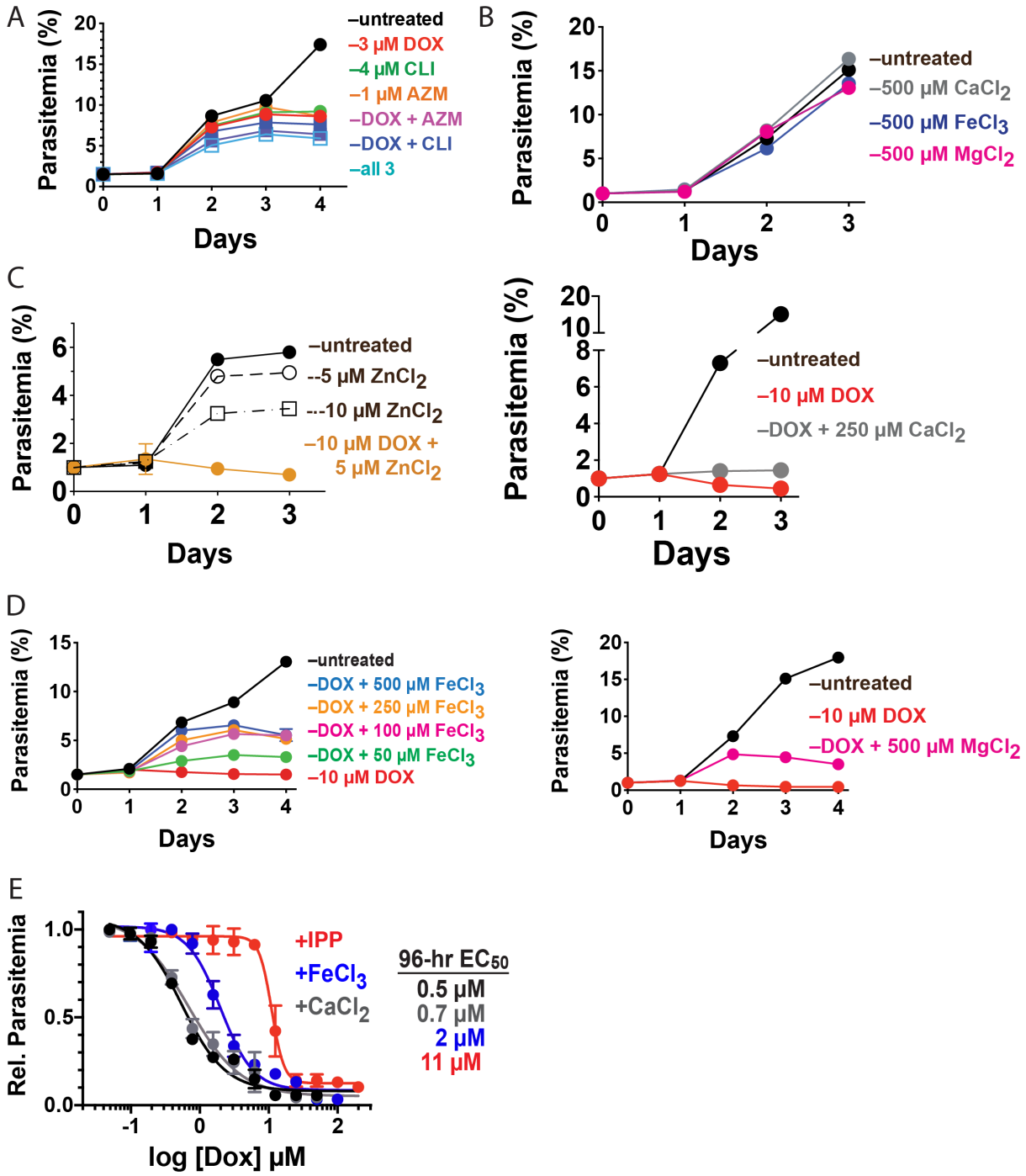

Figure 3- figure supplement 1. Additional, independent growth assays with DOX, other antibiotics, and metals. Additional continuous growth assays of synchronized Dd2 parasites treated with (A) DOX, clindamycin (CLI), and/or azithromycin (AZM); (B) 500 µM of $CaCl_2$, $MgCl_2$, or $FeCl_3$ alone; (C) 10 µM DOX and 5 µM $ZnCl_2$ or 250 µM $CaCl_2$; (D) 10 µM DOX treated with 50 - 500 µM $FeCl_3$ or 500 µM $MgCl_2$. Individual data points are the ave ± sd from 2-4 biological replicates. (E) 96-hour growth-inhibition assays for DOX-treated D10 parasites in the absence or presence of 200 µM IPP, 500 µM $FeCl_3$, or 500 µM $CaCl_2$. Parasites were synchronized by magnet purification of schizonts followed by 5-hour incubation with uninfected erythrocytes and treatment with 5% D-sorbitol. Data points are the ave ±sd of 3 biological replicates.

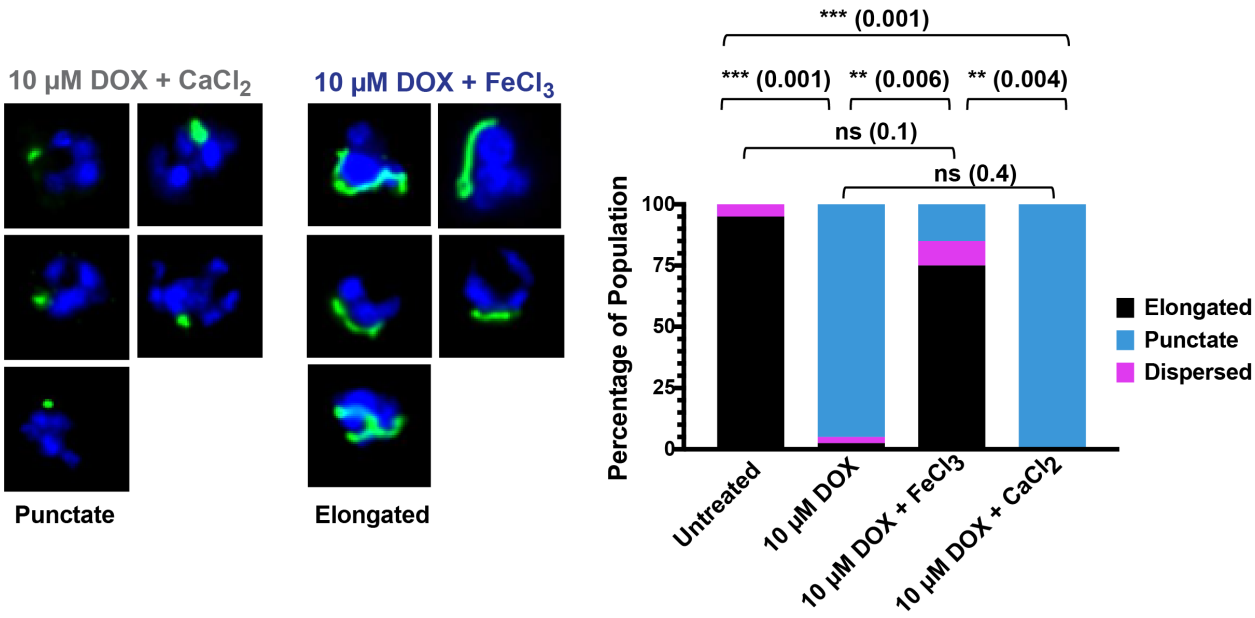

Figure 3- figure supplement 2. Additional epifluorescence images of D10 parasites treated with DOX and metals. Magnet plus sorbitol-synchronized parasites were treated as rings with 10 µM DOX ±500 µM $FeCl_3$ or $CaCl_2$ and imaged 36 hours later (green = ACP_L-GFP, blue = nuclear Hoechst stain). 20-40 parasites were examined for each treatment condition on each given day for duplicate experiments, and data were plotted as the average percentage of parasites in each population that displayed an elongated, punctate, or dispersed apicoplast GFP signal. For clarity, error bars are not displayed but standard deviations were <10% in all conditions. Cell-percentage differences were analyzed by unpaired t-test (P values in parentheses, ns = not significant).

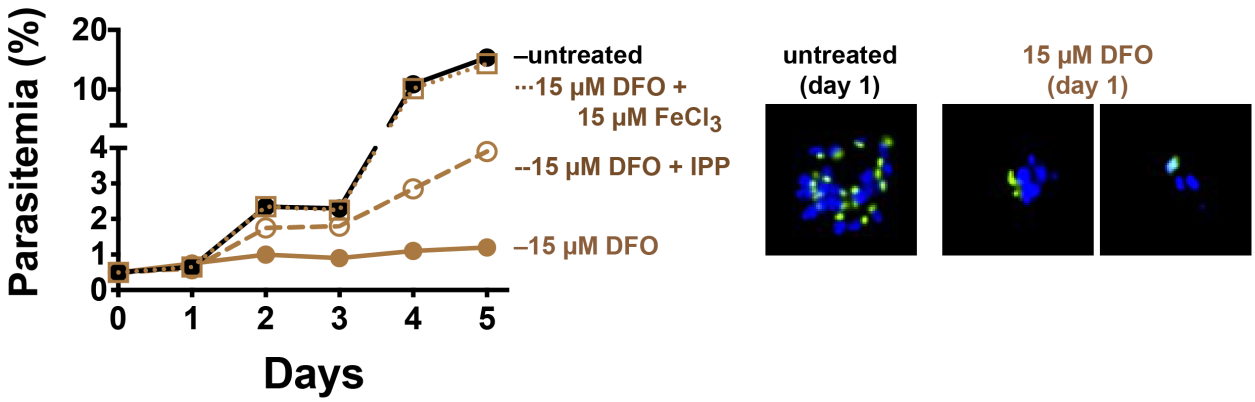

Figure 3- figure supplement 3. Effect of deferoxamine on parasite growth and apicoplast biogenesis. (Left) Continuous growth assay of synchronized Dd2 parasites cultured without or with 15 µM deferoxamine (DFO), 15 µM $FeCl_3$, or 200 µM IPP. (Right) Fluorescence microscopy of live, synchronized D10 parasites untreated or treated with 15 µM DFO and imaged 36 hours later (green = ACP_L-GFP, blue = nuclear Hoechst stain).